Available online at www.sciencedirect.com
SCIENCE DIRECT
International Journal of Machine Tools & Manufacture 45 (2005) 1531–1541
INTERNATIONAL JOURNAL OF MACHINE TOOLS & MANUFACTURE DESIGN, RESEARCH AND APPLICATION
www.elsevier.com/locate/ijmactool

Tooth profile design for the manufacture of helical gear sets with small numbers of teeth

Chien-Fa Chen[a], Chung-Biau Tsay[b,*]

[a]Department of Mechanical Engineering, National United University, Miaoli 36003, Taiwan, ROC
[b]Department of Mechanical Engineering, National Chiao Tung University, Hsinchu 30010, Taiwan, ROC

Received 16 June 2004; accepted 13 January 2005
Available online 11 May 2005

Abstract

Based on gear theory and generating mechanism, this investigation presents a complete mathematical model of a helical gear set with small number of teeth. The unavoidable tooth-profile undercutting of the gears with small number of teeth is examined by using the developed mathematical model and the conventional method of tooth-profile shifting. Furthermore, an alternative method for lessening the tooth-profile undercutting is also presented by considering a modification of the basic fillet geometry using a modified rack cutter. A third method, combining the aforementioned two methods for the design of helical gears with small number of teeth is also proposed to yield a gear set without tooth undercutting. The mating gear with profile shifting is generated using the pinion as a shaper. The tip fillet and root fillet are modified and a clearance between the pinion and the mating gear is also included in the design. Analysis results indicate that the change of distance between the centers of gear set depends only on gear shifting. Moreover, computer graphs are demonstrated the profile-shifted and the proposed modified gear tooth profiles.

Keywords: Undercutting; Modified tooth surface; Small number of teeth; Profile shifting

1. Introduction

It is known that spur and helical gears with small number of teeth may exhibit tooth undercutting. Gears with small number of teeth are typically not used in power transmissions. However, helical gears are extensively used in industry, and may be generated by hobs, shapers and rack cutters. Several researchers [1–5] and AGMA publications [6,7] have significantly contributed to the design and manufacturing of this type of gearing. Many researchers have also studied gear design and manufacturing with tooth-profile shifting. Ishibashi et al. [8] derived a mathematical model of the spur gear with two or three pinion teeth, according to the basic geometry. Their mathematical model was used to investigate the design, manufacture and load capacity. Ishibashi and Yoshino [9] also determined the load capacity of Novikov gears with three to five pinion teeth. Additionally, Komori et al. [10] developed a spur gear with LogiX tooth profiles which have zero relative curvature at many contact points. Arikan [11] determined the maximum possible contact ratios using an *x*-zero gear pair for spur gears with small number of teeth. Analysis results were also compared with addendum modification coefficients recommended by ISO.

Tooth undercutting occurs at the generated gear tooth surfaces, under certain conditions, such as small number of teeth, small pressure angles and negatively shifted profiles. If tooth undercutting occurs, the tooth thickness near the gear fillets is reduced and the gear bending moment capacity is also decreased. Mabie and Reinholtz [12] considered geometric relationships to study the tooth undercutting of spur gears generated by shaper cutters. Many researchers [13,14] studied tooth undercutting for various types of gearing. Litvin [15,16] presented a detailed theory of the gear non-undercutting conditions. Tsai and Tsai [17] proposed a method of designing high-contact-ratio spur gears with quadratic parametric tooth profiles, that have a short addendum without tooth undercutting.

* Corresponding author. Tel./fax: +886 3 572 8450.
E-mail address: cbtsay@mail.nctu.edu.tw (C.-B. Tsay).

0890-6955/$ - see front matter © 2005 Elsevier Ltd. All rights reserved.
doi:10.1016/j.ijmachtools.2005.01.017

Nomenclature

a_i	tool setting of rack cutter generating the involute gear ($i=0, 1$)
e	total profile shifting coefficient
e_i	profile shifting coefficient ($i=1, 2, p, g$)
C	clearance of the mating gears
E	center distance of the mating gears (or shaper and generated gear)
E'	operating center distance of the mating gears
$[L_{ij}]$	projection transformation matrix (from S_j to S_i)
l	surface parameter of rack cutter (in mm)
$[M_{ij}]$	coordinate transformation matrix (from S_j to S_i)
m_{12}	gear ratio
m_n	normal module of the gear
$\mathbf{n}_i^{(j)}$	unit normal vector of rack cutter surface j ($j=1$, 2 and 3, which represent part 1, 2 and 3 of rack cutter normal section (Fig. 1), respectively) represented in coordinate system i ($i=c, a$)
$\mathbf{n}_1^{(j)}$	unit normal vector of generated gear surface j ($j=1\sim3$)
$\boldsymbol{R}_i^{(j)}$	position vector of surface j ($j=1$, 2 and 3, which represent part 1, 2 and 3 of rack cutter normal section (Fig. 1), respectively, and their corresponding generated gear tooth surfaces) represented in coordinate system i ($i=1, 2, c, a$)
r	distance between gear rotational center and beginning point of modified region (in mm)
r_i	radius of pitch circle of pinion and gear ($i=1, 2$) (in mm)
r_j	radius of centrode of pinion and gear ($j=p, g$) (in mm)
r_r	radius of the modified root fillet of shaper (in mm)
r_t	radius of the modified tip fillet of shaper (in mm)
S_i	coordinate system i ($i=1, 2, a, c, h$)
$\mathbf{T}$	tangent vector to a curve
T_i	number of teeth of pinion and gear ($i=1, 2$)
$x_i^{(j)}$, $y_i^{(j)}$, $z_i^{(j)}$	position vector of modified fillet surface j ($j=r, t$ where r represents root fillet and t indicates tip fillet) represented in coordinate system i ($i=1, 2$)
u	surface parameter of rack cutter (in mm)
$\mathbf{V}_{tr}^{(c1)}$	transfer velocity of the contact point
$\mathbf{V}_r^{(1)}$	relative velocity of the contact point with the gear
$\mathbf{V}_r^{(c)}$	relative velocity of the contact point with the rack cutter
Σ_a	normal section of rack cutter surface
Σ_e	rack cutter surface
ψ_{bs}	operating pressure angle of helical gear
ψ_n	normal pressure angle of rack cutter (in degrees)
ψ_s	transverse pressure angle helical gear
ρ_i	radius of tip and root fillets of rack cutter ($i=0$, 1) (in mm)
θ_n	variable parameter of root fillet of rack cutter (in degrees)
ζ_n	variable parameter of tip fillet of rack cutter (in degrees)
ϕ_i	rotational angle of pinion and gear ($i=1, 2$) (in degrees)
λ	lead angle of gear (in degrees)
σ_i	spanned angle of modified root and tip fillet ($i=r, t$) (in degrees)

Tooth undercutting may reduce the gear strength and contact ratio. Undercutting is therefore an important problem in gear design. Of course, tooth undercutting can be eliminated by increasing teeth to the gear. However, the use of more teeth is occasionally not allowable. This study aims to obtain a spur or helical gear with small number of teeth, without tooth undercutting. Based on the gear theory and the gear generating mechanism, a mathematical model of the helical gear has been developed. Moreover, the condition for gear non-undercutting is also derived by considering the relative velocity between the rack cutter and the gear blank, and by considering the differentiated equation of meshing. The conventional tooth-profile shifting method is used to solve the tooth undercutting problem. Nevertheless, this method always increases the tooth thickness of the fillets and reduces the contact ratios. An alternative method, which considers the modification of fillet geometry, is presented to develop a gear set without tooth undercutting. Based on the tooth-profile shifting and the basic fillet geometry modification methods, a third method that combines these two methods is presented to obtain a gear set with a higher contact ratio and fillet strength without tooth undercutting. Furthermore, the use of a modified pinion with modified tip fillets is proposed to generate the mating gear pair and thus prevents the occurrence of singular points on the generated gear tooth. In such a generation process, tooth-profile shifting and gear clearance have also been considered. Finally, a computer program is developed to generate the complete geometry of the gear, including the involute tooth surfaces, the modified root fillets and the modified tip fillets. Results of this study can be used to design not only spur and helical gears with small number of teeth, but also one-stage high contact ratio gear pairs. Consequently, the total volume of the gearbox can be reduced, the structure of the gear transmission mechanism can be simplified and the gear assembly can also be made easier. Besides, the cost of a on-stage gearbox is cheaper than that of the multi-stage gearbox.

2. Mathematical model of the modified tooth surface

2.1. Rack cutter surfaces

Fig. 1 depicts the normal section of rack cutter Σ_a used to generate involute helical gears. Part 1 of the tip fillet of the generating rack cutter is an arc of radius ρ_0, which generates the root fillet of the gear; part 2 of the tool profile is a straight line $\overline{M_0M_2}$ that generates the involute profile of the gear, and part 3 of the bottom fillet of the generating rack cutter is an arc of radius ρ_1, which generates the tip fillet of the gear. The position vector of the straight line $\overline{M_0M_2}$ of the rack cutter normal section can be represented in the coordinate system $S_a(X_a,Y_a,Z_a)$ by the following equations.

$$\boldsymbol{R}_a^{(2)} \begin{bmatrix} l\cos\psi_n - a_0 \\ \pm(l\sin\psi_n - a_0\tan\psi_n - b_0) \\ 0 \end{bmatrix}, \quad 0 \le l \le (a_0 + a_1)/\cos\psi_n. \tag{1}$$

Similarly, the equation of the tip fillet of the normal section of the generating rack cutter can be expressed as follows:

$$\boldsymbol{R}_a^{(1)} = \begin{bmatrix} -a_0 + \rho_0\sin\psi_n - \rho_0\sin\zeta_n \\ \pm(-a_0\tan\psi_n - b_0 - \rho_0\cos\psi_n + \rho_0\cos\zeta_n) \\ 0 \end{bmatrix}, \quad \psi_n < \zeta_n < \pi/2. \tag{2}$$

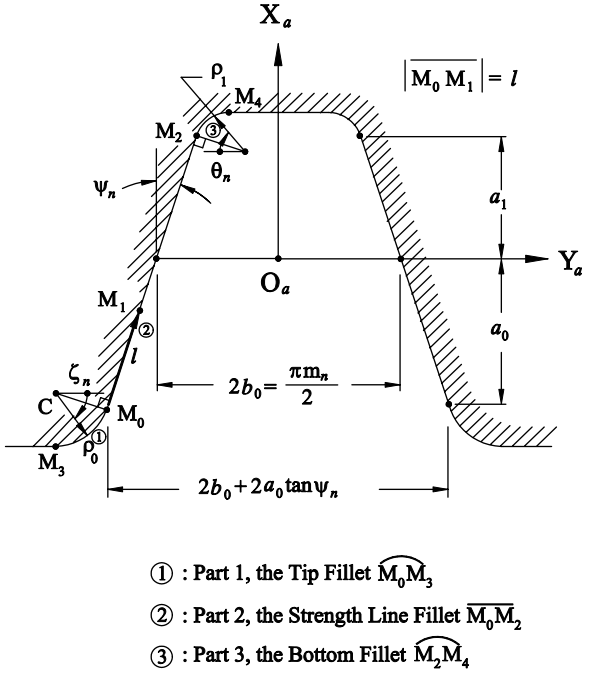

Fig. 1. Normal section of rack cutter Σ_a.

The equation of the bottom fillet of the generating rack cutter normal section are as follows.

$$\boldsymbol{R}_a^{(3)} = \begin{bmatrix} a_1 - \rho_1\sin\psi_n + \rho_1\sin\theta_n \\ \pm(a_1\tan\psi_n - b_0 + \rho_1\cos\psi_n - \rho_1\cos\theta_n) \\ 0 \end{bmatrix}, \quad \psi_n < \theta_n < \pi/2. \tag{3}$$

The upper signs in Eqs. (1)–(3) refer to the left-side of the rack cutter normal section while the lower signs refer to the right-side of the rack cutter normal section. l, ζ_n, and θ_n are the design parameters of the rack cutter surface that determine the location of points on the straight line, tip fillet, and bottom fillet, respectively.

In simulating the rack cutter surface for the helical gear generation, the normal section of the rack cutter Σ_a, attached to the coordinate system S_a with its origin O_a, is translated along the line $\overline{O_aO_c}$ as shown in Fig. 2. Therefore, $u = |\overline{O_aO_c}|$ is also one of the design parameters of the rack cutter surface, and λ is the lead angle of the generated helical gear. The rack cutter surface Σ_c for helical gear generation can be represented in the coordinate system $S_c(X_c,Y_c,Z_c)$ by applying the following homogeneous coordinate transformation matrix equation:

$$\boldsymbol{R}_c^{(i)} = [M_{ca}]\boldsymbol{R}_a^{(i)}, \tag{4}$$

where

$$[M_{ca}] = \begin{bmatrix} 1 & 0 & 0 & 0 \\ 0 & \sin\lambda & \cos\lambda & u\cos\lambda \\ 0 & -\cos\lambda & \sin\lambda & u\sin\lambda \\ 0 & 0 & 0 & 1 \end{bmatrix},$$

and $i = 1$, 2 and 3. Substituting Eq. (1) into Eq. (4), enables the position vector of the rack cutter surface Σ_c traced out by the straight line $\overline{M_0M_2}$ (part 2 in Fig. 1), to be represented in coordinate system S_c as

$$\boldsymbol{R}_c^{(2)} = \begin{bmatrix} l\cos\psi_n - a_0 \\ \pm(l\sin\psi_n - a_0\tan\psi_n - b_0)\sin\lambda + u\cos\lambda \\ \mp(l\sin\psi_n - a_0\tan\psi_n - b_0)\cos\lambda + u\sin\lambda \end{bmatrix}. \tag{5}$$

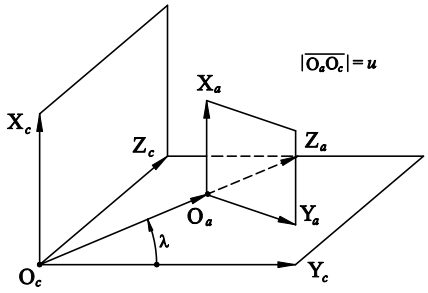

Fig. 2. Formation of rack cutter surface Σ_c for helical gear generation.

Based on the differential geometry, the unit normal vectors of the above-mentioned rack cutter surface represented in coordinate system S_c are

$$\mathbf{n}_c^{(i)} = \frac{\frac{\partial \boldsymbol{R}_c^{(i)}}{\partial l} \times \frac{\partial \boldsymbol{R}_c^{(i)}}{\partial u}}{\left| \frac{\partial \boldsymbol{R}_c^{(i)}}{\partial l} \times \frac{\partial \boldsymbol{R}_c^{(i)}}{\partial u} \right|}. \tag{6}$$

2.2. Generated tooth surfaces

Fig. 3 illustrates the relationship between rack cutter Σ_c and generated gear of the gear generation mechanism. In deriving equations for the gear tooth surface, the coordinate systems $S_c(X_c,Y_c,Z_c)$, $S_1(X_1,Y_1,Z_1)$ and $S_h(X_h,Y_h,Z_h)$ are attached to the rack cutter, generated gear and gear housing, respectively. Based on gear theory, the generated gear surface can be obtained by simultaneously considering the locus of the imaginary rack cutter represented in coordinate system S_1 and the equation of meshing [3,15,16] of the cutter and the generated gear. Thus, the mathematical model of the gear tooth surface is

$$\boldsymbol{R}_1^{(i)} = [M_{1c}]\boldsymbol{R}_c^{(i)}, \tag{7}$$

and

$$\frac{X_c^{(i)} - x_c^{(i)}}{n_{cx}^{(i)}} = \frac{Y_c^{(i)} - y_c^{(i)}}{n_{cy}^{(i)}} = \frac{Z_c^{(i)} - z_c^{(i)}}{n_{cz}^{(i)}}, \tag{8}$$

where

$$[M_{1c}] = \begin{bmatrix} \cos\phi_1 & -\sin\phi_1 & 0 & r_1(\cos\phi_1 + \phi_1 \sin\phi_1) \\ \sin\phi_1 & \cos\phi_1 & 0 & r_1(\sin\phi_1 - \phi_1 \cos\phi_1) \\ 0 & 0 & 1 & 0 \\ 0 & 0 & 0 & 1 \end{bmatrix}.$$

Symbols $X_c^{(i)}$, $Y_c^{(i)}$ and $Z_c^{(i)}$ represent the coordinates of a point on the instantaneous axis of gear rotation I−I in coordinate system S_c; $x_c^{(i)}$, $y_c^{(i)}$ and $z_c^{(i)}$ are coordinates of the instantaneous contact point on the rack cutter surface Σ_c; and $n_{cx}^{(i)}$, $n_{cy}^{(i)}$ and $n_{cz}^{(i)}$ are the direction cosines of the rack cutter surface unit normal $\mathbf{n}_c^{(i)}$. Substituting Eqs. (5) and (6) into Eq. (8), yields the equation of meshing for the rack cutter and generated gear.

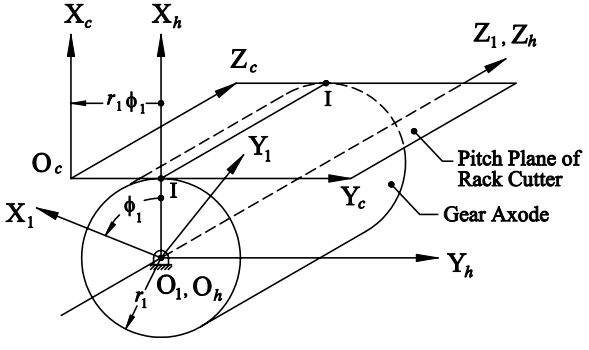

Fig. 3. Coordinate relationship between rack cutter and generated gear.

$$f_1(l,u,\phi_1) = \pm\left(\frac{a_0}{\cos\psi_n} + b_0\sin\psi_n - l\right)\sin\lambda + (r_1\phi_1 - u\cos\lambda)\sin\psi_n = 0. \tag{9}$$

Substituting Eqs. (5) and (9) into Eq. (7) yield the generated helical gear with involute profile tooth surface as follows:

$$\begin{aligned} x_1^{(2)} &= (l\cos\psi_n - a_0 + r_1)\cos\phi_1 \mp (a_0 - l\cos\psi_n)\cot\psi_n \sin\lambda \sin\phi_1, \\ y_1^{(2)} &= (l\cos\psi_n - a_0 + r_1)\sin\phi_1 \pm (a_0 - l\cos\psi_n)\cot\psi_n \sin\lambda \cos\phi_1, \quad \text{and} \\ z_1^{(2)} &= \pm(a_0 - l\cos\psi_n)\cot\psi_n \tan\lambda \sin\lambda \pm \left(\frac{a_0\tan\psi_n + b_0 - l\sin\psi_n}{\cos\lambda}\right) + r_1\phi_1\tan\lambda. \end{aligned} \tag{10}$$

The following matrix equation gives the unit normal of the tooth surface.

$$\mathbf{n}_1^{(i)} = [L_{1c}]\mathbf{n}_c^{(i)}, \tag{11}$$

where

$$[L_{1c}] = \begin{bmatrix} \cos\phi_1 & -\sin\phi_1 & 0 \\ \sin\phi_1 & \cos\phi_1 & 0 \\ 0 & 0 & 1 \end{bmatrix}.$$

2.3. Tooth undercutting analysis

At any instantaneous contact point of the rack cutter and generated gear, the absolute velocities of the rack cutter and generated gear are the same. Nevertheless, the absolute velocity can be decomposed into components, the relative velocity $\mathbf{V}_r^{(c)}$ and $\mathbf{V}_r^{(1)}$ and transfer velocity $\mathbf{V}_{tr}^{(c)}$ and $\mathbf{V}_{tr}^{(1)}$ of the rack cutter and generated gear, respectively. Therefore,

$$\mathbf{V}_r^{(c)} + \mathbf{V}_{tr}^{(c)} = \mathbf{V}_r^{(1)} + \mathbf{V}_{tr}^{(1)}, \quad \text{or} \quad \mathbf{V}_r^{(c)} + \mathbf{V}_{tr}^{(c)} - \mathbf{V}_{tr}^{(1)} = \mathbf{V}_r^{(c)} + \mathbf{V}_{tr}^{(c1)} = \mathbf{V}_r^{(1)}. \tag{12}$$

When tooth undercutting occurs, a singular point appears on the generated gear tooth surface and its surface tangent $\mathbf{T}=0$ at this singular point. The mathematical definition of singularity of the generated gear can be represented in coordinate system S_c by equation $\mathbf{V}_r^{(1)} = 0$. Therefore, Eq. (12) becomes

$$\mathbf{V}_r^{(c)} + \mathbf{V}_{tr}^{(c1)} = 0. \tag{13}$$

Recalling Fig. 3, the conditions under which a singular point may appear on the working surface of the helical gear generated by the straight line (line $\overline{M_0M_2}$ shown in Fig. 1) of the rack cutter are considered here. The relative tranfer velocity between the gear blank and the rack cutter,

represented in coordinate system S_c, can be obtained as follows:

$$\mathbf{V}_c^{(c1)} = \omega_1 \begin{bmatrix} r_1\phi_1 - y_c^{(2)} \\ x_c^{(2)} \\ 0 \end{bmatrix}. \tag{14}$$

Notably, Eq. (5) specified the position vector of the rack cutter surface, $\boldsymbol{R}_c^{(2)}$. Eq. (13) can thus be rewritten by

$$\frac{\partial \boldsymbol{R}_c^{(2)}}{\partial l}\frac{\mathrm{d}l}{\mathrm{d}t} + \frac{\partial \boldsymbol{R}_c^{(2)}}{\partial u}\frac{\mathrm{d}u}{\mathrm{d}t} = -\mathbf{V}_{\mathrm{tr}}^{(c1)}, \tag{15}$$

Differentiating the equation of meshing, Eq. (9), yields

$$\frac{\partial f_1}{\partial l}\frac{\mathrm{d}l}{\mathrm{d}t} + \frac{\partial f_1}{\partial u}\frac{\mathrm{d}u}{\mathrm{d}t} = -\frac{\partial f_1}{\partial \phi_1}\frac{\mathrm{d}\phi_1}{\mathrm{d}t}. \tag{16}$$

Eqs. (15) and (16) form a system of four linear equations in two unknowns, $\mathrm{d}l/\mathrm{d}t$ and $\mathrm{d}u/\mathrm{d}t$. This system of equations has a unique solution for the unknowns if the matrix

$$A = \begin{bmatrix} \dfrac{\partial \boldsymbol{R}_c^{(2)}}{\partial l} & \dfrac{\partial \boldsymbol{R}_c^{(2)}}{\partial u} & -\mathbf{V}_{\mathrm{tr}}^{(c1)} \\ \dfrac{\partial f_1}{\partial l} & \dfrac{\partial f_1}{\partial u} & -\dfrac{\partial f_1}{\partial \phi_1}\dfrac{\mathrm{d}\phi_1}{\mathrm{d}t} \end{bmatrix} \tag{17}$$

has a rank of two. This yields the following four determinants equal zero:

$$\Delta_1 = \begin{vmatrix} \dfrac{\partial x_c^{(2)}}{\partial l} & \dfrac{\partial x_c^{(2)}}{\partial u} & -V_{x,\mathrm{tr}}^{(c1)} \\ \dfrac{\partial y_c^{(2)}}{\partial l} & \dfrac{\partial y_c^{(2)}}{\partial u} & -V_{y,\mathrm{tr}}^{(c1)} \\ \dfrac{\partial f_1}{\partial l} & \dfrac{\partial f_1}{\partial u} & -\dfrac{\partial f_1}{\partial \phi_1}\dfrac{\mathrm{d}\phi_1}{\mathrm{d}t} \end{vmatrix} = 0, \tag{18}$$

$$\Delta_2 = \begin{vmatrix} \dfrac{\partial x_c^{(2)}}{\partial l} & \dfrac{\partial x_c^{(2)}}{\partial u} & -V_{x,\mathrm{tr}}^{(c1)} \\ \dfrac{\partial z_c^{(2)}}{\partial l} & \dfrac{\partial z_c^{(2)}}{\partial u} & -V_{z,\mathrm{tr}}^{(c1)} \\ \dfrac{\partial f_1}{\partial l} & \dfrac{\partial f_1}{\partial u} & -\dfrac{\partial f_1}{\partial \phi_1}\dfrac{\mathrm{d}\phi_1}{\mathrm{d}t} \end{vmatrix} = 0, \tag{19}$$

$$\Delta_3 = \begin{vmatrix} \dfrac{\partial y_c^{(2)}}{\partial l} & \dfrac{\partial y_c^{(2)}}{\partial u} & -V_{y,\mathrm{tr}}^{(c1)} \\ \dfrac{\partial z_c^{(2)}}{\partial l} & \dfrac{\partial z_c^{(2)}}{\partial u} & -V_{z,\mathrm{tr}}^{(c1)} \\ \dfrac{\partial f_1}{\partial l} & \dfrac{\partial f_1}{\partial u} & -\dfrac{\partial f_1}{\partial \phi_1}\dfrac{\mathrm{d}\phi_1}{\mathrm{d}t} \end{vmatrix} = 0, \tag{20}$$

and

$$\Delta_4 = \begin{vmatrix} \dfrac{\partial x_c^{(2)}}{\partial l} & \dfrac{\partial x_c^{(2)}}{\partial u} & -V_{x,\mathrm{tr}}^{(c1)} \\ \dfrac{\partial y_c^{(2)}}{\partial l} & \dfrac{\partial y_c^{(2)}}{\partial u} & -V_{y,\mathrm{tr}}^{(c1)} \\ \dfrac{\partial z_c^{(2)}}{\partial l} & \dfrac{\partial z_c^{(2)}}{\partial u} & -V_{z,\mathrm{tr}}^{(c1)} \end{vmatrix} = 0. \tag{21}$$

Eq. (21) is the same as the equation of meshing, and it is satisfied since the points of tangency of the rack cutter and the generated tooth surfaces are considered. Thus, only Eqs. (18)–(20) should be applied to determine the conditions of singularity for the generated tooth surface. Therefore, a sufficient condition for the occurrence of a singularity of the generated tooth surface is

$$G(l, u, \phi_1) = \Delta_1^2 + \Delta_2^2 + \Delta_3^2 = 0. \tag{22}$$

Eq. (22) yields the condition of tooth undercutting as follows:

$$l = \frac{1}{\cos\psi_n}\left(a_0 - \frac{r_1 \sin^2\psi_n}{B}\right), \tag{23}$$

where

$$B = \sin^2\psi_n + \cos^2\psi_n \sin^2\lambda.$$

2.4. Generating nonstandard gears by rack cutters

Nonstandard gears can be generated by a standardized tool used for generation of standard gears but with modified tool settings with respect to the gear being generated. Usually, modified tool settings are applied to prevent tooth undercutting of the generated gear. Referring to Fig. 4 and Eq. (23), the rack cutter will not undercut the gear tooth if the following inequality is satisfied.

$$\frac{e_p m_n}{\cos\psi_n} \geq |l| = \left|\frac{1}{\cos\psi_n}\left(a_0 - \frac{r_1 \sin^2\psi_n}{B}\right)\right|. \tag{24}$$

Thus, the normal shifting coefficient of the rack cutter setting e_p, which corresponds to gear tooth non-undercutting is

$$e_p \geq \left|\frac{a_0}{m_n} - \frac{T_1}{2\sin\lambda}\frac{\sin^2\psi_n}{B}\right|, \tag{25}$$

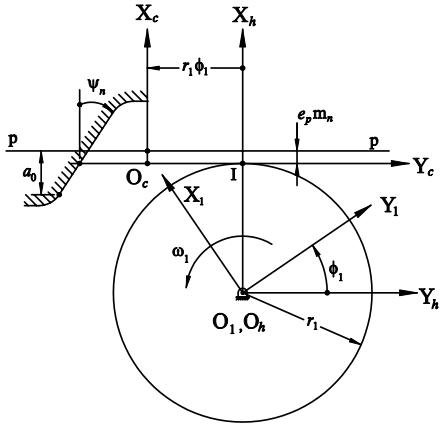

Fig. 4. Nonstandard gears generated by a rack cutter.

Table 1
Some major design parameters for helical gears with small number of teeth

Parameters	Pinion	Gear	Notes
Normal module m_n	1.75 mm/teeth		Given
Pressure angle	20°		
Lead angle	60°		
Teeth number	2	60	
Shifting coefficient $e_1=0.7$, $e_2=0.7$	$e_p=e_1=0.7$	$e_g=-e_1+e_2=-1.4$	
Total shifting coefficient	$e=e_p+e_g=e_2=-0.7$		Calculated
Center distance	61.106 mm		
l corresponding to undercutting	0.236 mm		
l corresponding to point C	0.246 mm		
Radius of root fillet r_r	1.045 mm		
Spanned angle of root fillet σ_r	$-60.14°\le\sigma_r\le0°$		
Clearance C	0.4 mm		
Radius of tip fillet r_t	0.332 mm		
Spanned angle of tip fillet σ_t	$0°\le\sigma_t\le26.69°$		

where T_1 represents the number of teeth on the generated gear; m_n is the normal module, and a_0 is the standardized parameter of the rack cutter, as shown in Fig. 1.

Example 1. Nonstandard gears generated by different profile shifting coefficients.

Table 1 lists some important design parameters for helical gears with small number of teeth. Fig. 5 plots the profiles of the pinion with shifting coefficients e_p of 0.5 and 1.0. Tooth undercutting on the gear root is found to be reduced by increasing the profile shifting coefficient. However, the thickness of the gear tooth is increased compared with the standard gear for nonstandard gears.

3. Modification of the root fillet surfaces of the pinion

In a one-stage gear set with a high gear ratio, one of the gears must be extremely small. Tooth undercutting on the gear root may occur when the small number of teeth are used. This work proposes a modified curvilinear root profile, rather than an ordinary gear root profile, to improve the bending strength of the pinion root. Fig. 6 shows the cross section of the pinion tooth surface on plane $z_1=0$ mm. Since tooth undercutting occurs on the involute profile of the generated pinion tooth surface, the mathematical model of the involute profile (refer to Eq. (10)) of the first quadrant is expressed as follows:

$$\begin{aligned} x_1 &= (l\cos\psi_n - a_0 + r_1)\cos\phi_1 - (l\cos\psi_n \\ &\quad - a_0)\cot\psi_n \sin\lambda\sin\phi_1, \\ y_1 &= (l\cos\psi_n - a_0 + r_1)\sin\phi_1 + (l\cos\psi_n \\ &\quad - a_0)\cot\psi_n \sin\lambda\cos\phi_1, \end{aligned} \tag{26}$$

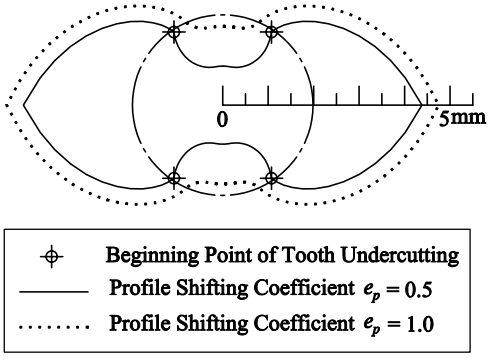

Fig. 5. Computer graph of the nonstandard gear.

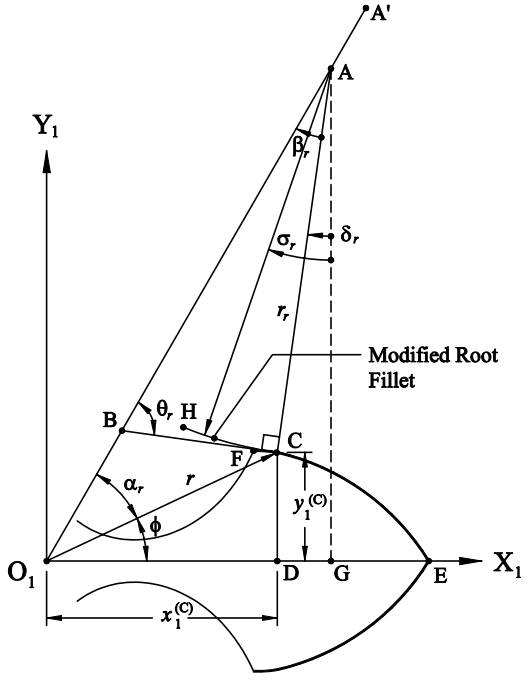

Fig. 6. Geometries of tooth undercutting and modified fillet.

and

$$z_1 = -(a_0 \tan\psi_n - l\sin\psi_n)\cos\lambda + \left(\frac{a_0}{\cos\psi_n \sin\psi_n} - \frac{l}{\sin\psi_n}\right)\tan\lambda \sin\lambda - \frac{b_0}{\cos\lambda} + r_1\phi_1 \tan\lambda.$$

Closely examining Fig. 6 reveals that the curve EF is an involute profile generated by the straight line of the rack cutter, and point F is the beginning point at which tooth undercutting occurs. Notably, the parameter l corresponding to point F can be obtained using Eq. (23). Consider a point C, which is close to point F, where the parameter l of the rack cutter profile (Fig. 1) that corresponds to point C slightly exceeds that of the rack cutter profile that corresponds to point F. $x_1^{(C)}$ and $y_1^{(C)}$ are the components of the line $\overline{O_1C}$ represented in coordinate system S_1 and are given by Eq. (26). An expression for the length $|\overline{O_1C}| = r$ should be derived firstly as follows:

$$r = \sqrt{(x_1^{(C)})^2 + (y_1^{(C)})^2} = \sqrt{r_1^2 - \frac{r_1^2 - [(l\cos\psi_n - a_0)(1+\cot^2\psi_n \sin^2\lambda) + r_1]^2}{1+\cot^2\psi_n \sin^2\lambda}}. \quad (27)$$

The line $\overline{BC}$ is the tangent to the involute curve EF at point C, while the line $\overline{AC}$ is the normal to the involute curve EF at point C. Angle $A'O_1E$ depends on the number of teeth T_1, and is expressed as follows:

$$\angle A'O_1E = \frac{\pi}{T_1}. \quad (28)$$

In this study, the length $\overline{AC}$ is the proposed radius of the modified root fillet: $|\overline{AC}| = r_r$. Applying the law of sine to triangle AO_1C yields the following equation:

$$\frac{r_r}{\sin\alpha_r} = \frac{r}{\sin\beta_r}. \quad (29)$$

Differentiating Eq. (26) yields the tangent vector to the involute profile at point C

$$\mathbf{T} = \frac{dx_1}{dl}\mathbf{i}_1 + \frac{dy_1}{dl}\mathbf{j}_1. \quad (30)$$

According to Eq. (28), the unit vector of the slope of line $\overline{O_1A}$ is

$$\mathbf{m} = \cos\frac{\pi}{T_1}\mathbf{i}_1 + \sin\frac{\pi}{T_1}\mathbf{j}_1. \quad (31)$$

Taking the dot product of vectors $\mathbf{T}$ and $\mathbf{m}$ yields the angle formed by lines $\overline{BA}$ and $\overline{BC}$:

$$\theta_r = \cos^{-1}\frac{\left(\cos\frac{\pi}{T_1}\right)\frac{dx_1}{dl} + \left(\sin\frac{\pi}{T_1}\right)\frac{dy_1}{dl}}{\sqrt{\left(\frac{dx_1}{dl}\right)^2 + \left(\frac{dy_1}{dl}\right)^2}}. \quad (32)$$

According to Fig. 6, the angle β_r equals $\pi/2 - \theta_r$. Substituting β_r into Eq. (29) yields the radius r_r of the modified root fillet.

With reference to Fig. 6, the modified circular arc CH with a radius of r_r and a center at point A is proposed for the modified root fillet when the pinion exhibits serious tooth undercutting. The screw motion of the modified circular arc performs the helical pinion root-fillet surface. Consequently, the cross sections of the helicoids corresponding to $z_1 = 0$ and $z_1 =$ constant, represent the same plane curve in two positions. One cross section coincides with the other after a rotation about the z_1 axis through an angle η in a screw motion. The proposed modified root fillet of the pinion can be represented in coordinate system S_1 as follows.

$$\begin{aligned} x_1^{(r)} &= x_1^{(C)}\cos\eta \mp y_1^{(C)}\sin\eta + r_r\sin(\delta_r \pm \eta) - r_r\sin(\sigma_r \pm \eta),\\ y_1^{(r)} &= x_1^{(C)}\sin\eta \pm y_1^{(C)}\cos\eta \mp r_r\cos(\delta_r \pm \eta) \pm r_r\cos(\sigma_r \pm \eta),\\ \text{and } z_1^{(r)} &= r_1\eta\tan\lambda, \end{aligned} \quad (33)$$

where $\delta_r = \frac{\pi}{2} - \frac{\pi}{T_1} - \beta_r$, $\delta_r \le \sigma_r \le \delta_r + \beta_r$, and σ_r represents the spanned angle of the modified root fillet.

4. Modification of the tip fillet surface of the shaper

The pointed teeth are an important issue in gear design and manufacture, especially for helical gears with small number of teeth. Since the gear teeth are generated by a pinion-type shaper, the tip fillet of the shaper must be considered to avoid the occurrence of singular points in the generation process. Fig. 7 depicts the cross section of the shaper on the plane $z_1 = 0$ mm. Point J is the beginning point of the tip fillet that lies on the involute profile, and the coordinates of point J are $x_1^{(J)}$ and $y_1^{(J)}$; point K is the point of intersection of the X_1 axis and the vector $\mathbf{T}$ that is tangent to the involute tooth profile at

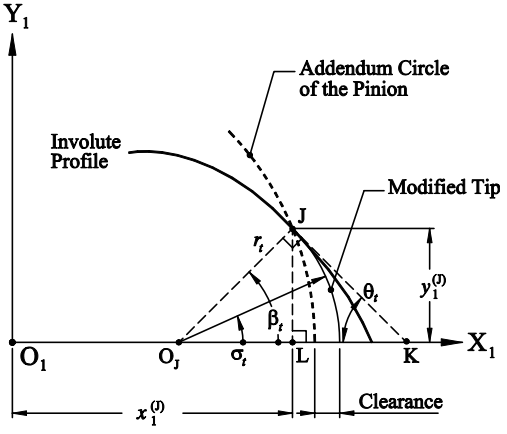

Fig. 7. Modified tip fillet of the shaper.

point J. O_J is the point of intersection of the X_1 axis and the normal vector that is perpendicular to the involute profile at point J, and point O_J is also the center of the modified tip fillet. The length $\overline{O_JJ}$ is the proposed radius of the modified tip fillet, $|\overline{O_JJ}| = r_t$. Eq. (26) determines the coordinates of point J. Following the procedure similar to that of previous section, the angle formed by the axis X_1 and line $\overline{JK}$ can be expressed by

$$\theta_t = \cos^{-1} \frac{\frac{dx_1}{dl}}{\sqrt{\left(\frac{dx_1}{dl}\right)^2 + \left(\frac{dy_1}{dl}\right)^2}}. \tag{34}$$

According to Fig. 7, angle β_t equals $\pi/2 - \theta_t$. Applying the law of sine to triangle JO_JL yields the radius of the modified tip fillet, $r_t = y_1^{(J)}/\sin\beta_t$.

Similarly, the proposed modified tip fillet of the shaper can be represented in coordinate system S_1 as follows:

$$\begin{aligned} x_1^{(t)} &= x_1^{(J)} \cos\eta - r_t \cos\beta_t \cos\eta + r_t \cos(\sigma_t \mp \eta), \\ y_1^{(t)} &= x_1^{(J)} \sin\eta - r_t \cos\beta_t \sin\eta \mp r_t \sin(\sigma_t \mp \eta), \\ \text{and} \quad z_1^{(t)} &= r_1 \eta \tan\lambda \end{aligned} \tag{35}$$

where σ_t is the spanned angle of the modified tip fillet and $0 \le \sigma_t \le \beta_t$.

The radius of the modified tip fillet, r_t, is determined by the location of point J. Point J is selected as the point that at which the modified tip fillet makes a clearance between the addendum of the pinion and the dedendum of the generated gear, as shown in Fig. 7. AGMA's fundamental formula for the recommended clearance of fine pitch gears is suggested as follow:

$$C = 0.2m_n + 0.05, \tag{36}$$

where C represents the clearance and m_n is the normal module of the gear.

5. Mathematical model of the gear generated by shapers

Fig. 8 displays the kinematic relationship between the shaper and the generated gear. Coordinate systems $S_1(X_1,Y_1,Z_1)$ and $S_2(X_2,Y_2,Z_2)$ are rigidly attached to the shaper cutter and the gear, respectively. The position vector of the shaper cutter can be transformed from coordinate system S_1 to S_2 by applying the following homogeneous coordinate transformation matrix equation.

$$\boldsymbol{R}_2^{(i)} = [M_{21}]\boldsymbol{R}_1^{(i)}, \tag{37}$$

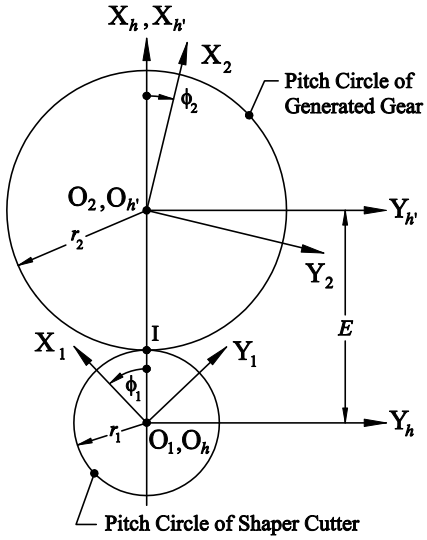

Fig. 8. Kinematic relationship between the shaper and generated gear.

where

$$[M_{21}] = \begin{bmatrix} \cos(\phi_1+\phi_2) & \sin(\phi_1+\phi_2) & 0 & -E\cos\phi_2 \\ -\sin(\phi_1+\phi_2) & \cos(\phi_1+\phi_2) & 0 & E\sin\phi_2 \\ 0 & 0 & 1 & 0 \\ 0 & 0 & 0 & 1 \end{bmatrix},$$

and E is the center distance between the shaper and the generated gear. The equation of meshing between the shaper and the generated gear is

$$\frac{X_1^{(i)} - x_1^{(i)}}{n_{1x}^{(i)}} = \frac{Y_1^{(i)} - y_1^{(i)}}{n_{1y}^{(i)}} = \frac{Z_1^{(i)} - z_1^{(i)}}{n_{1z}^{(i)}}, \tag{38}$$

where $X_1^{(i)}$, $Y_1^{(i)}$ and $Z_1^{(i)}$ are coordinates of the instantaneous contact point I, and $x_1^{(i)}$, $y_1^{(i)}$, $z_1^{(i)}$ and $n_{1x}^{(i)}$, $n_{1y}^{(i)}$, $n_{1z}^{(i)}$ are the coordinates and the normal vector components of an instantaneous point on the shaper profile, respectively, represented in coordinate system S_1. According to gear theory, the profile of a generated gear can be obtained by simultaneously considering the equation of meshing and the loci of the shaper cutter represented in the gear's coordinate system. Thus, the involute gear profile generated by the shaper (i.e. involute profile shown in Fig. 7) is expressed as follows:

$$\begin{aligned} x_2^{(2)} &= (l\cos\psi_n - a_0 + r_1)\cos\phi_2 \\ &\quad \pm (a_0 - l\cos\psi_n)\cot\psi_n \sin\lambda \sin\phi_2 - E\cos\phi_2, \\ y_2^{(2)} &= -(l\cos\psi_n - a_0 + r_1)\sin\phi_2 \pm (a_0 - l\cos\psi_n) \\ &\quad \times \cot\psi_n \sin\lambda \cos\phi_2 + E\sin\phi_2 \quad \text{and} \\ z_2^{(2)} &= \pm (a_0 - l\cos\psi_n)\cot\psi_n \tan\lambda \sin\lambda \\ &\quad \pm \left(\frac{a_0\tan\psi_n + b_0 - l\sin\psi_n}{\cos\lambda}\right) + r_1 m_{12}\phi_2 \tan\lambda, \end{aligned} \tag{39}$$

where $m_{12} = \frac{T_2}{T_1} = \frac{\phi_1}{\phi_2}$.

Similarly, the modified gear root fillet generated by the modified tip of the shaper (Fig. 7) can be represented as follows:

$$\begin{aligned} x_2^{(t)} &= (x_1^{(J)} - r_t \cos\beta_t)\cos(\phi_1+\phi_2-\eta) \\ &\quad + r_t \cos[\sigma_r \mp(\eta-\phi_1-\phi_2)] - E\cos\phi_2, \\ y_2^{(t)} &= -(x_1^{(J)} - r_t \cos\beta_t)\sin(\phi_1+\phi_2-\eta) \\ &\quad \mp r_t \sin[\sigma_r \mp(\eta-\phi_1-\phi_2)] + E\sin\phi_2, \\ z_2^{(t)} &= r_1\eta\tan\lambda, \end{aligned} \tag{40}$$

and

$$f_2^{(t)} = -r_1\sin(\sigma_t \mp\eta\pm\phi_1) + (x_1^{(J)} - r_t\cos\beta_t)\sin\sigma_t = 0. \tag{41}$$

Similarly, the modified gear tip fillet generated by the modified root fillet of the shaper (Fig. 6) is as follows:

$$\begin{aligned} x_2^{(r)} &= x_1^{(C)}\cos(\phi_1+\phi_2-\eta) \pm y_1^{(C)}\sin(\phi_1+\phi_2-\eta) \\ &\quad + r_r\sin[\delta_r \pm(\eta-\phi_1-\phi_2)] \\ &\quad - r_r\sin[\sigma_r \pm(\eta-\phi_1-\phi_2)] - E\cos\phi_2, \\ y_2^{(r)} &= -x_1^{(C)}\sin(\phi_1+\phi_2-\eta) \pm y_1^{(C)}\cos(\phi_1+\phi_2-\eta) \\ &\quad \mp r_r\cos[\delta_r \pm(\eta-\phi_1-\phi_2)] \\ &\quad \pm r_r\cos[\sigma_r \pm(\eta-\phi_1-\phi_2)] + E\sin\phi_2, \\ z_2^{(r)} &= r_1\eta\tan\lambda, \end{aligned} \tag{42}$$

and

$$\begin{aligned} f_2^{(r)} &= -r_1\cos(\sigma_r \pm\eta\mp\phi_1) + x_1^{(C)}\cos\sigma_r + y_1^{(C)}\sin\sigma_r \\ &\quad + r_r\sin(\delta_r-\sigma_r) = 0. \end{aligned} \tag{43}$$

6. Designing a nonstandard gear generated by shapers

The center distance of gear pairs depends on the profile-shifting coefficient. The total profile-shifting coefficient of the gear pairs is $e=e_p+e_g$ when the profile-shifting coefficients are e_p and e_g for the pinion and gear, respectively. Thus, the operating center distance [16] is

$$E' = \frac{(r_1+r_2)\cos\psi_s}{\cos\psi_{bs}}, \tag{44}$$

where ψ_s is the transverse pressure angle, and the operating pressure angle, ψ_{bs}, is given by the following involute function [16].

$$\mathrm{inv}\psi_{bs} = 2\tan\psi_s\left(\frac{e_p+e_g}{T_1+T_2}\right) + \mathrm{inv}\psi_s, \tag{45}$$

where e_p and e_g represent the normal profile shifting coefficients of the rack cutter and the generated gear, respectively, and T_1 and T_2 represent the number of teeth of the pinion and gear. The involute function can be alternatively expressed as follows [16].

$$\mathrm{inv}\psi_{bs} = \tan\psi_{bs} - \psi_{bs}. \tag{46}$$

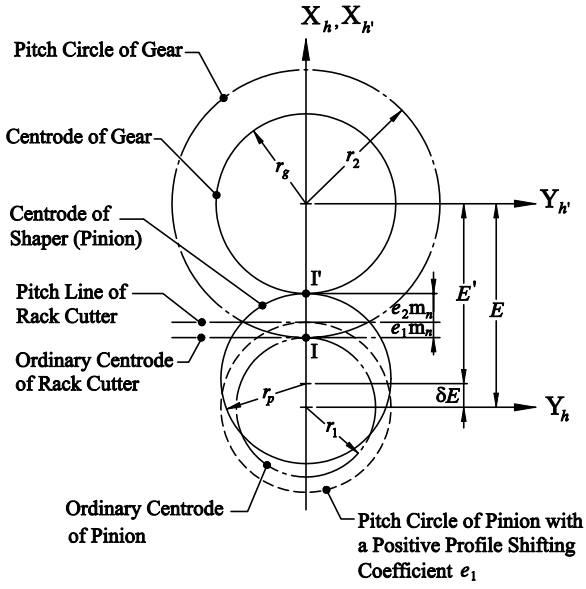

Fig. 9. Visualization of profile shifting.

The operating center distance can be obtained by substituting Eqs. (45) and (46) into Eq. (44). Notably, the operating center distance depends on the sum of profile shifting coefficients. Fig. 9 presents the profile shifting relationship of the pinion and the gear during their generation. The pinion is generated using a rack cutter with a positive profile shifting coefficient $e_p=e_1$, and then using the pinion as the shaper (i.e. the same pinion-type shaper) to generate the mating gear with a negative profile shifting coefficient e_2. This generating procedure changes the instantaneous center of rotation from point I to point I′, such that the profile shifting coefficient of the generated gear is $e_g=-e_1+e_2$. Hence, the total profile shifting coefficient of the mating gear pair is $e=e_p+e_g=e_2$. Restated, the change of the center distance depends only on the profile shifting coefficient e_2. The change of center distance does not impact the gear ratio m_{12}, but does affect the radii of pinion and gear centrodes. The new pitch radii of the pinion and the gear [16] are

$$r_p = \frac{E'}{1+m_{12}} \text{ and } r_g = \frac{E'}{1+1/m_{12}}. \tag{47}$$

Example 2. Computer graphs of the pinion and gear with profile shifting coefficients.

Table 1 lists the major parameters of the pinion and gear. Table 1 also shows all other corresponding design parameters calculated according to the proposed tip and fillet modification method. Based on the developed pinion and gear mathematical models expressed in Eqs. (10), (33) and (39)–(47), Fig. 10 displays the computer graphs of the pinion and the gear with profile shifting and modified tooth surfaces.

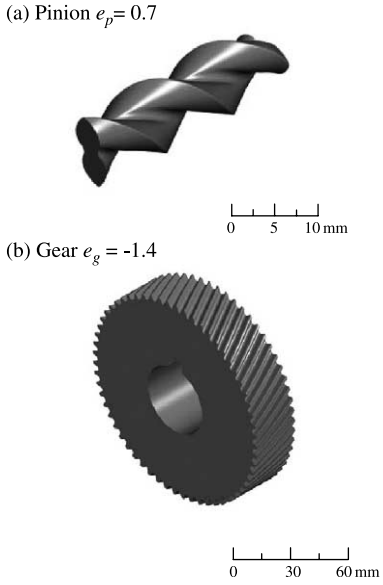

Fig. 10. Computer graphs of the pinion and gear with profile shifting and modified tooth surface.

7. Discussion

The conventional method of applying positive profile-shifted cutting is widely used in industry to manufacture helical gears with small number of teeth, to avoid tooth undercutting. However, positive profile-shifted cutting causes the increase of gear fillet thickness as the number of teeth decreases. The increase of fillet thickness results in the decrease of gear addendum. This study proposes an alternative method that modifies the geometry of the fillet. A third method, combining the profile-shifted cutting and fillet modification, is also proposed, to yield an improved result. Fig. 11 compares the tooth profiles of the pinion obtained by applying the methods of the tooth-profile shifting and the combination of profile-shifted cutting and tooth fillet modification, respectively. The parameters are the same as those shown in Table 1. Differences between the tooth surfaces obtained by these two methods are observed.

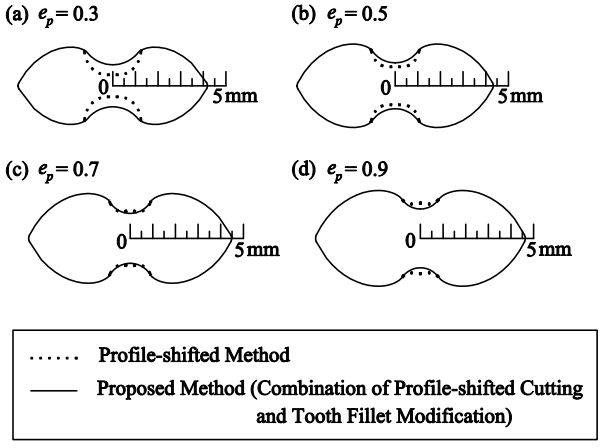

Fig. 11. Comparisons on profile-shifted and modified tooth profiles.

Applying the positive profile-shifting coefficients with values of 0.3 and 0.5 reduces but does not eliminate the tooth undercutting problem, when the tooth-profile shifting method is applied. According to Fig. 11, when the shifting coefficient equals 0.7, the tooth profiles generated by these two methods are very similar. When the shifting coefficient equals 0.9, the generated root fillets of the profile-shifted pinion are higher than those generated by the combination of profile shifting and tooth modification method. In other words, by applying the conventional profile-shifted method, an increase in the shifting coefficient leads to a decrease of the gear addendum, and thus reducing the gear contact ratio. Furthermore, the change of the center distance between the pinion and the gear depends on the profile shifting coefficient of the shaper when the gear is generated by shapers according to the proposed method. According to the simulated results, a combination of the tooth modification method and the tooth-profile shifting method can solve the tooth undercutting problem. Additionally, the clearance between the pinion and the gear can be determined during the gear generation process. According to the proposed method, the change of the center distance depends only on gear shifting coefficient when the gear is generated by shapers. Mathematical models developed in this study can be used in designing spur and helical gear sets with small number of teeth. Fig. 12 displays the pinion and the gear that designed and manufactured by

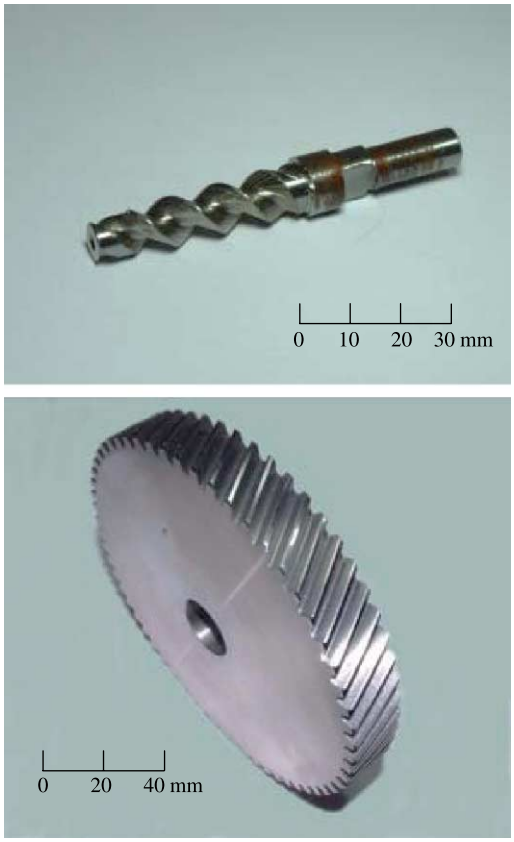

Fig. 12. Pinion and gear with profile shifting and modified tooth surface.

using the proposed method and the gear pair has already been used to a motor-driven wheelchair.

8. Conclusion

A mathematical model of the modified helical gear with small number of teeth has been developed by tooth-profile shifting and basic geometry modification. The condition of tooth undercutting for the involute profile gears has been investigated using the developed mathematical models. Computer graphs of the pinion and gear profiles generated by various methods are displayed for comparison. Figs. 10, 11 and 12 have shown the verification and validation of the proposed methods and their corresponding gear tooth mathematical models. The proposed methods and developed mathematical models of the modified helical gear can be helpful to facilitate to design and manufacture of spur and helical gears with small number of teeth.

References

[1] E. Buckingham, Analytical Mechanics of Gears, Dover Publications Inc, New York, 1949.
[2] D.W. Dudley, Practical Gear Design, McGraw-Hill Book Co, New York, 1982.
[3] F.L. Litvin, C.B. Tsay, Helical gears with circular arc teeth: simulation of conditions of meshing and bearing contact, Transactions of the ASME, ASME Journal of Mechanisms Transmissions Automation Design 107 (1985) 556–564.
[4] F.L. Litvin, Methods for generation of gear tooth surface and basic principals of computer aided tooth contact analysis, Proceeding of Computers in Engineering 1 (1985) 556–564.
[5] J.R. Colbourne, The Geometry of Involute Gears, Springer, New York, 1987.
[6] AGMA, Information Sheet-Geometry Factors for Determining the Strength of Spur, Helical, Herringbone and Bevel Gear Teeth. AGMA, 226.01, 1970.
[7] AGMA, Design Guide for Vehicle Spur and Helical Gears. AGMA, 170.01, 1976.
[8] A. Ishibashi, H. Yoshino, I. Nakashima, Design and manufacturing processes and load carrying capacity of cylindrical gear pairs with 2 to 4 pinion teeth for high gear ratios (1st report design and manufacture and surface durability of gears with 2 to 3 pinion teeth), Transactions of the Japan Society of Mechanical Engineers, Series C 47 (416) (1981) 507–515.
[9] A. Ishibashi, H. Yoshino, Design, manufacture and load carrying capacity of Novikov gears with 3–5 pinion teeth for high gear ratios (1st report, design, manufacture and power transmission efficiency), Transactions of the Japan Society of Mechanical Engineers, Series C 49 (447) (1983) 2039–2047.
[10] T. Komori, Y. Ariga, S. Nagata, A new gears profile having zero relative curvature at many contact points (LogiX Tooth Profile), Transactions of the ASME, Journal of Mechanical Design 112 (1990) 430–436.
[11] M.A.S. Arikan, Determination of maximum possible contact ratios for spur gear drives with small number of teeth, Proceedings of the ASME Design Technical Engineering Conferences 82 (1) (1995) 569–576.
[12] H.H. Mabie, C.F. Reinholtz, Mechanisms and Dynamics of Machinery, 4th ed., Wiley, New York, 1987.
[13] V. Kin, Limitation of Worm and Worm gear surfaces in order to avoid undercutting, Gear Technology 1990; 33–35.
[14] Z.H. Fong, C.B. Tsay, The undercutting of circular-cut spiral bevel gears, Transactions of the ASME, ASME Journal of Mechanical Design 114 (1992) 317–325.
[15] F.L. Litvin, Theory of Gearing, NASA Publication RP-1212, Washington DC, 1989.
[16] F.L. Litvin, Gear Geometry and Applied Theory, Prentice-Hall, New Jersey, 1994.
[17] M.H. Tsai, Y.C. Tsai, Design of high-contact-ratio spur gears using quadratic parametric tooth profiles, Mechanism and Machine Theory 33 (5) (1998) 551–564.